Gradient-based Multi-objective Design Optimisation Formulation of Grid-connected Wound-rotor Induction Motors

M. Mabhula, *Student Member, IEEE* and M. J. Kamper, *Senior Member, IEEE*

***Abstract*—In this paper, a gradient-based multi-objective optimisation of the grid-connected wound-rotor induction motor is achieved by using quality modelling and a computationally efficient procedure. The procedure combines two objective functions, namely torque and efficiency, into a single-objective function of a sum of squared residual errors. It is shown that using the proposed computationally efficient optimisation method greatly improves the torque and efficiency of the motor, which is shown to also come with a good power factor. The obtained optimum solution is reliable, as the accuracy of the motor performance model has been validated by experimental test results. The optimisation method can be applied to a many-to-single objective function design optimisation, and thus overall represents a beneficial to electrical machine optimisation.**

***Index Terms*—design optimisation, modified method of feasible direction, modelling, induction motor, wound-rotor.**

I. Introduction

With the increase in energy demand, there are many efforts to solve this demand, amongst others by attaining energy from renewable energy sources and improving the energy efficiency of the load. The bulk of electrically generated energy today is converted to mechanical energy by means of induction motors (IMs) [1]. Of these IMs, the wound-rotor induction motor (WRIM) is used in large power-conversion (MW range) applications such as mine motor crushers. Hence, energy-efficiency design approaches in these large motor systems will go a long way in improving the energy scenario.

Modern design and modelling approaches of WRIMs have improved steadily over the years and have, to some extent, helped to reduce some of the uncertainties associated with IM designs [2], [3]. Prescribed optimisation algorithms are readily available and could make a significant contribution to improved IM design. The reason the contribution of these optimisation algorithms has been moderate lies in the modest quality of the WRIM models, which lie at the core of a successful design. Using a machine model of modest accuracy, it cannot be expected to find a truly optimal design [4]. Furthermore, conventional gradient-optimisation algorithms themselves have problems associated with local rather than global solutions and their dependence on initial parameter values [5]. In this respect, the genetic algorithms circumvent these issues, however, at the expense of increased computation times [6].

Although the power factor is not a true energy-savings measure, improving the power factor improves the system energy efficiency and reduces energy cost if the end-user is subjected to utility power factor charges [7]. IMs reduce plant power factors [8], so in this respect it is important to have good IM power factors. On the other hand, it is the overall plant power factor that counts and there are ways of correcting low-system power factors [9], [10]. Hence, a high IM power factor is not vitally important, specifically if the IM's power factor is not affecting much the overall system power factor. The issue of high-power-factor IMs is the significant increase in motor manufacturing cost. Furthermore, [11] found that, by focussing on a high power factor does not necessarily lead to a good IM design. In this respect, it is much better to focus on efficiency in the design of the IM, which has been shown also leads to relatively good power factors. The IM designer indeed has to consider a number of objectives in the IM design, of which at most about two can be put forward in a multi-objective design optimisation to obtain a Pareto front from which the designer can choose a design.

In this paper, the aim is to make a further contribution to the optimum design of grid-connected WRIMs. The reason for the focus on the WRIM is the still competitive performance versus cost provided by the WRIM in high-power level (MW power range) applications, and the advantage of the rotor-winding accessibility compared to cage-rotor technology [8]. In the design optimisation, an IM model of high accuracy, such as the one demonstrated in [4], is used and focuses specifically on a method of using a gradient-based optimisation algorithm to find the true optimum design of the WRIM.

II. Optimal design problem function

The IM optimal design problem function constitutes of three mathematically formulated design functions namely:

- objective functions;
- constraint functions; and
- design variables.

The objective and constraint functions are required performance candidates and the functions to be either maximised or minimised respectively. Both functions depend on

This work was supported by Stellenbosch University, South Africa.

M. Mabhula and M. J. Kamper are with the Department of Electrical and Electronic Engineering, Stellenbosch University, Stellenbosch, South Africa (e-mail: mabhulamkhululi@gmail.com, kamper@sun.ac.za).

978-1-7281-9944-3/20/$31.00 ©2020 IEEE

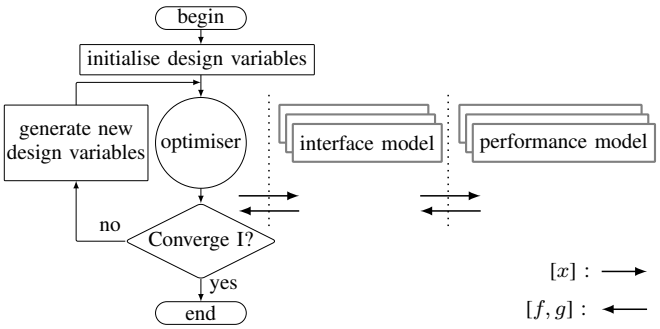

Fig. 1. IM flow chart of optimisation procedure coupled directly with computationally efficient models.

the design variables. Mathematically, the general non-linear multi-variable constrained performance-optimisation problem function can be defined as [12]:

Find the design variables

$$x_1, x_2, \ldots, x_K \tag{1}$$

such that the objective functions

$$f_m(x_1, x_2, \ldots, x_i) \quad m = 1, 2, \ldots, M \tag{2}$$

are minimum (maximum) subject to constraints functions

$$\begin{aligned} g_n(x_1, x_2, \ldots, x_i) &= 0 \qquad n = 1, 2, \ldots, n_e \\ g_n(x_1, x_2, \ldots, x_i) &\leqslant 0 \qquad n = (n_e + 1), \ldots, N \end{aligned} \tag{3}$$

and lower x_k^l and upper x_k^u boundary conditions

$$x_k^l \leqslant x_k \leqslant x_k^u \qquad k = 1, 2, \ldots, K. \tag{4}$$

III. Optimisation procedure

To solve the defined optimisation problem (1)-(4), the procedure used in this paper is not only to use a computationally efficient performance calculation model, but also a quality interface model with the optimiser, as illustrated in Fig. 1. The interface model plays an essential role in the usability of the performance model information by the optimiser, which is a significant contribution to the location of the optimal design of the motor. The interface model is discussed in the next section.

Following Fig. 1, the evaluated objective $[f]$ and constraint $[g]$ function values are read in the first call of the optimiser, using initial design variable values $[x]$ passed to and from the performance model through the interface model. The optimiser is either a gradient- (e.g. modified method of feasible direction, MMFD) or a non-gradient (e.g. non-dominated sorting genetic algorithm, NSGA-II) based optimisation algorithm. In both scenarios, the optimiser control parameters are explained well in [13]. Depending on the optimiser, the other prime operators passed to the optimiser are the lower x^l and upper x^u bounds of the design variables, population, and maximum or minimum number of iterations. The optimiser reads all these design variable and constraint function values, including their upper and lower bounds. The process from the performance model is repeated with new design variables from the optimiser until the desired routine control parameters are satisfied, i.e. Converge I shown in Fig. 1.

IV. Interface model

In addition to the designer's skill, the interface model, shown in Fig. 1, is crucial to the quality improvement of the model that lies at the core of the optimiser and helps the optimiser locate the global optimal solution.

To model the interface model, following on the problem (1)-(4), the design variables are defined in matrix form as

$$[x] = [x_1 \quad x_2 \quad \ldots \quad x_K]^T, \tag{5}$$

where T is the transpose operator. During the optimisation procedure of Fig. 1, the optimiser assumes each design variable holds an equal weight and does not take into account the relative importance of the individual variable. To take into account the relative importance of the individual variable and avoiding the domination of one variable by the other in satisfying the optimum solution, thereby giving unsatisfactory results, the technique of smoothing the problem function is adapted. The latter is achieved by strengthening or weakening some of the design variables to restrict them to falling within a given range seen by the optimiser. Thus, in an arbitrary given range of bounds (0 to 1) generally seen by the optimiser, the scaled design variable is defined by

$$x'_k = (x_k - x_k^{min})/(x_k^{max} - x_k^{min}), \tag{6}$$

where the prime superscript denotes a scaled parameter. In (6), max and min denote maximum and minimum actual values of the corresponding scaled parameter, which depends on the designer's skill. Furthermore, following function scaling of (6), the actual design variables x_k from the scaled values x'_k in the bounds 0 to 1 can then be determined easily. The procedure in (5) and (6) described above is also followed for the objective and constraint functions of the interface model.

Although multi-objective optimisation using non-gradient-based optimisers like NSGA-II [6] provides much more information and insight into the problem function, it is also possible to combine multi-objectives into a single-objective optimisation using gradient-based optimisers like MMFD [14] to save search times. The latter is implemented during the optimisation process in the interface model by utilising the sum of the squared residual errors. The residual errors are left by a set of objective function values not satisfying a set of targeted objective function values. It is these residual errors of each objective function value that define the combined multi-objective effect of objective functions to a single objective (sum of squared residual errors), resulting in

$$f_{\mathrm{R}} = \sum_{m=1}^{M} \epsilon_m^2, \quad \epsilon_m = \begin{cases} 0 & : f_m \geqslant f_m^{min} \\ \dfrac{f_m^{min} - f_m}{f_m^{min}} & : f_m < f_m^{min}, \end{cases} \tag{7}$$

for f_m no less than f_m^{min}. The set value of f_m^{min} defines the minimal objective function value. In (7), it is only necessary to utilise penalty functions if the optimisation package does not have an option of built-in constraints.

Furthermore, unlike NSGA-II, MMFD has a problem associated with local solutions rather than global solutions and the dependence on their starting or initial design variables [6]. To resolve this delinquent, the technique of different starting design variable is utilised in certain cases. In each case (C1, C2, C3), the problem function is defined from (4) using three different initial design variable vectors as

$$\text{C1: } [x] = \begin{bmatrix} x_k^l \\ \vdots \\ x_K^l \end{bmatrix} \text{ C2: } [x] = \begin{bmatrix} x_k^a \\ \vdots \\ x_K^a \end{bmatrix} \text{ C3: } [x] = \begin{bmatrix} x_k^u \\ \vdots \\ x_K^u \end{bmatrix}, \quad (8)$$

where x_k^l and x_k^u are defined in (4) and $x_k^a = 0.5(x_k^l + x_k^u)$. The optimum case resulting from (8) is then transferred to the next starting design variables of the problem function of (7) and optimised. The latter is repeated until there is no significant change in the optimum results. Besides scaling design parameters and using different starting design variables, minimum and maximum bounds are included with the constraints to avoid valid but undesirable results.

V. Performance model

In addition to the quality of the interface model discussed in Section IV, a further challenge is to determine the motor performance computational efficiently; with powerful computers, solving complex problems with maximum speed, computational efficient nowadays increasingly means energy efficient.

It is important to state that not only is a performance calculation model of modest accuracy crucial for the optimal design of IMs, but also for the compatibility of the model. For that, the FEM-based computationally efficient parameter and performance model in [4] is adapted. That is to say, the accessibility of any parameter of the IM, e.g. inductances and torque components, during the optimisation procedure provides a bigger platform for the designer to different optimisation options, which is not available in commercial classic models.

Following Fig. 1, the performance model is used to evaluate the objective $[f]$ and constraint $[g]$ functions of defined design variables $[x]$ passed from the optimiser through the quality interface model. This is done by using a method of solving for the excitation currents at a grid-defined voltage operating point, and using the solved currents to calculate the motor performance, i.e. $[f]$ and $[g]$. The performance model takes into account the effects of saturation since, for the economic use of the lamination material, IMs are operated near saturation or sometimes deeply saturated.

A. Solving excitation currents

The key feature of the FEM used in this paper is that, in its basic form, requires defined currents, whereas the grid-connected IM under study relates to a defined voltage. Hence,

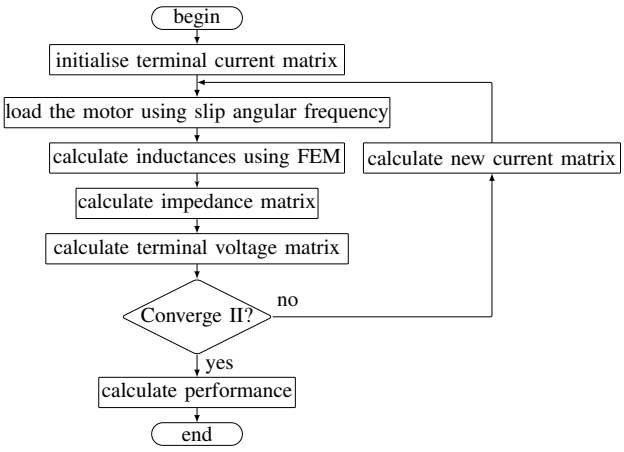

Fig. 2. Grid-connected IM flow chart of the performance model.

FEM currents are solved with reference to the defined grid-voltage using the iterative processes as illustrated in Fig. 2. Following Fig. 2, using a magneto-static non-linear 2D FEM for a given initial current matrix (stator and rotor currents) and slip angular frequency (or rotor position), the magnetic field is obtained, and then total-phase main-flux linkages are calculated. In 2D problems, the corresponding magneto-static Maxwell equations are solved in the FEM by finding the vector potential which satisfies the input current density. The phase flux linkages calculated from the found vector potential are transformed into dq-axes flux linkages. Using the total dq-axes main-flux linkages given by

$$\begin{aligned} \Lambda_{dms} &= L_{dsds}I_{ds} + L_{dsqs}I_{qs} + L_{dsdr}I_{dr} + L_{dsqr}I_{qr} \\ \Lambda_{qms} &= L_{qsds}I_{ds} + L_{qsqs}I_{qs} + L_{qsdr}I_{dr} + L_{qsqr}I_{qr} \\ \Lambda_{dmr} &= L_{drds}I_{ds} + L_{drqs}I_{qs} + L_{drdr}I_{dr} + L_{drqr}I_{qr} \\ \Lambda_{qmr} &= L_{qrds}I_{ds} + L_{qrqs}I_{qs} + L_{qrdr}I_{dr} + L_{qrqr}I_{qr}, \end{aligned} \quad (9)$$

the FEM-based frozen permeability method is utilised to calculate the inductance parameters (L) of (9) [4].

The terminal voltage matrix is calculated from the impedance $[Z]$ and the initial current $[I]$ matrices as

$$[V] = [Z][I], \quad (10)$$

where $[V] = [V_{ds}\ V_{qs}\ V_{dr}\ V_{qr}]^T$, $[I] = [I_{ds}\ I_{qs}\ I_{dr}\ I_{qr}]^T$ and $[Z]$ is a 4×4 matrix of motor parameters. Thus, knowing the inductance parameters of (9), the main-winding resistance (R_m), end-winding resistance (R_e), inductance (L_e), and grid (ω_s) and slip (ω_Δ) angular frequencies, the impedance matrix is given by

$$[Z] = \begin{bmatrix} (R_s - \omega_s L_{qsds}) & -\omega_s(L_{qsqs} + L_{es}) & -\omega_s L_{qsdr} & -\omega_s L_{qsqr} \\ \omega_s(L_{dsds} + L_{es}) & (R_s + \omega_s L_{dsqs}) & \omega_s L_{dsdr} & \omega_s L_{dsqr} \\ -\omega_\Delta L_{qrds} & -\omega_\Delta L_{qrqs} & (R_r - \omega_\Delta L_{qrdr}) & -\omega_\Delta(L_{qrqr} + L_{er}) \\ \omega_\Delta L_{drds} & \omega_\Delta L_{drqs} & \omega_\Delta(L_{drdr} + L_{er}) & (R_r + \omega_\Delta L_{drqr}) \end{bmatrix}. \quad (11)$$

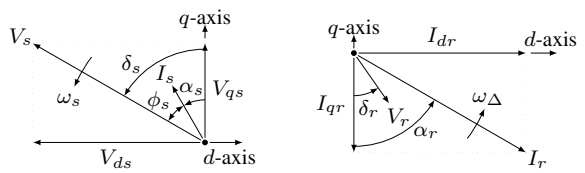

(a) (b)

Fig. 3. IM (a) stator and (b) rotor voltage and current relationship phasor diagram.

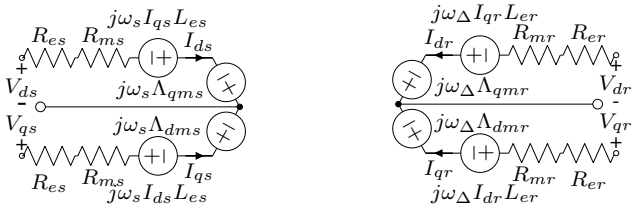

(a) (b)

Fig. 4. IM (a) stator and (b) rotor dq-axes equivalent circuit diagrams.

In (11), the stator and rotor end-winding inductances L_{es}, L_{er} are calculated as in [15]. The stator and rotor dc resistances (ignoring skin effect) are the sum of the main- and end-winding resistances calculated from the general formula, given by

$$R = R_m + R_e = w^2 pq(\ell_m + \ell_e)/\sigma cA. \tag{12}$$

In (12), w are winding-turns per slot, p are pole-pairs, q are slots per pole per phase, ℓ_m is the main conductor length (equal to stack length), ℓ_e is the end-winding length calculated as in [8], A is slot area, c is the slot fill factor calculated from the slot insulation, and σ is electric conductivity determined from a known temperature.

It is important to note that the voltages and currents of (10) are defined in the form of phasor components in space, as in Fig. 3. In Fig. 3, even though $V_r = 0$, it is shown as $V \neq 0$. This is so as to have a better understanding of how V_r zeros (IM rotor winding short-circulated) using the performance model in Fig. 2. Also using (10), Fig. 4 results, which are the dq-axes equivalent circuits referred to in the motor parameter calculation.

Following Fig. 2, the calculated terminal voltage matrix of (10) is compared to a defined grid and rotor voltage matrix, $[V_t]$. If not similar, new currents are calculated using the initial impedance and defined voltage matrices as

$$[I] = [Z]^{-1}[V_t]. \tag{13}$$

In (13), the defined grid and rotor voltage matrix is given by

$$[V_t] = [V_{dg} \quad V_{qg} \quad V_{d0} \quad V_{q0}]^T, \tag{14}$$

where V_{dq}, V_{qg} are the stator dq-axes' grid-voltages and $V_{d0} = V_{q0} = 0$ are the rotor dq-axes' short-circuitry voltages. The process described above is repeated iteratively, as shown in Fig. 2, until the voltage matrices of (10) and (14) are similar, i.e. Converge II is satisfied. At the point of convergence, the solved new currents of (13) are the required FEM currents for the performance calculation of the IM at the given grid voltage and load.

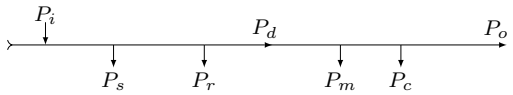

Fig. 5. IM simplified power-flow diagrams.

B. Calculation of objective and constraint functions

The performance model is for the calculation of objective and constraint functions needed for solving the optimisation problem function. After Converge II in Fig. 2, knowing the current and voltage matrices, the current densities (stator and rotor) and the power factor ($\cos(\phi_s)$ in Fig. 3) are easily computed from

$$J = w\sqrt{0.5(I_d^2 + I_q^2)}/cA, \tag{15}$$

and

$$\text{PF} = (V_{ds}I_{ds} - V_{qs}I_{qs})/\sqrt{(V_{ds}^2 + V_{qs}^2)(I_{ds}^2 + I_{qs}^2)}. \tag{16}$$

The percentage efficiency is calculated using the simplified power flow diagram of Fig. 5 as

$$\eta = (P_o/P_i) \times 100, \tag{17}$$

where the input power is given by

$$P_i = P_o + P_l. \tag{18}$$

The total losses P_l (excluding stray losses) in (18) are a sum of copper (stator P_s and rotor P_r), mechanical (P_m) and core losses (P_c). The output power in (17) is calculated from

$$P_o = P_d - (P_m + P_c), \tag{19}$$

where the developed power is given by

$$P_d = (\omega_s - \omega_\Delta)T_d. \tag{20}$$

In (20), T_d is the developed torque calculated from the stator total main flux linkages of (9) as

$$T_d = 1.5p(\Lambda_{dms}I_{qs} - \Lambda_{qms}I_{ds}), \tag{21}$$

and can be further decomposed into components using the inductance parameters of (9) for further IM analysis.

VI. Example of Optimisation Problem Application

The application example gives a multi-objective optimisation of a grid-connected, 4-pole, 400 V/50 Hz, 11 kW IM using the MMFD algorithm following the consideration given in the interface and performance models of Sections IV and V respectively. A general-purpose cage-rotor IM peripheral dimensions, D160M cast iron frame size, are referred to in this application example. Following the latter and other chosen design variables, Table I gives the fixed design variables. After fixing these design variables, the optimiser

TABLE I
DESIGN OPTIMISATION FIXED DESIGN VARIABLES

fixed design variable	symbol	value
stator and rotor slots per pole per phase (-)	q_s, q_r	3, 2
stator and rotor pole pairs (-)	p	2
stator and rotor phases (-)	–	3
stator and rotor slot fill factor (-)	c	0.4
stator and rotor stack length (mm)	ℓ_m	125
stator outer diameter (mm)	D_s	260
rotor inner diameter (mm)	d_r	60

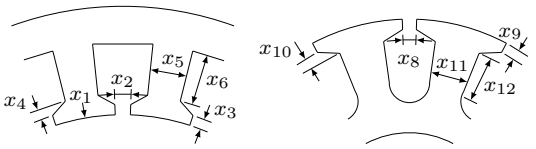

(a) (b)

Fig. 6. IM dimensional design variables of (a) stator and (b) rotor that are optimised.

TABLE II
DESIGN VARIABLES' FREEDOM OF MOVEMENT

variable	min	max	unit	variable	min	max	unit
x_1	145	184	mm	x_8	2	4.0	mm
x_2	1.5	4	mm	x_9	1.2	4.0	mm
x_3	1.0	4	mm	x_{10}	1.2	3	mm
x_4	1.0	3	mm	x_{11}	3.0	12	mm
x_5	3.0	12	mm	x_{12}	5.0	25.0	mm
x_6	5.0	25	mm	x_{13}	8	50	-
x_7	0.2	0.5	mm	x_{14}	0.0	25	rad/s

still has some freedom of movement over a restricted range of variables, such as stator and rotor slots, the air gap and bore diameter. Figure 6 shows the dimensional design variables to be optimised, with x_7 being the air-gap length. For the optimisation problem function, only fourteen dimensional variables are used, namely $x_1 - x_{12}$ of Fig. 6, and two additional variable, namely stator winding turns per slot x_{13} and slip angular frequency x_{14} (ω_Δ) are used, from (5) defined by

$$[x] = [x_1 \quad x_2 \quad \dots \quad x_{14}]^T. \tag{22}$$

In IMs, the air-gap flux density is inversely proportional to the number of turns [8]. Thus, increasing the stator turns results in lowering the average flux density. A reduction in average air-gap flux density results in a decrease in efficiency especially at higher loads on the IM, but can also improve the power factor. Hence, x_{13} (turns per slot) in (22) is selected as one of the design variables. The rotor turns are designed corresponding to the optimum stator turns for a specific voltage across the slip-rings. The variable x_{14} (slip angular frequency) in (22) is also selected to gain useful torque that increases continuously with the load and is necessary for torque production. The design variables freedom of movement space of (22) that are optimised following fixed variables in Table I, are given in Table II. The freedom of movement for x_{14} (ω_Δ) is according to IEC efficiency classes for a four-pole 11 kW IM [11].

As mentioned in the introduction, the relationship between maximum efficiency and other desirable characteristics of the IM is an aspect of energy conservation. Also, IM drives are commonly used for applications with a vast variation in mechanical load for torques under nominal values. Pumps, conveyors, blowers, fans and compressors are among these loads. Hence, the most ideal pattern for IM design should include efficiency improvement proportional to the load torque, such that optimal performance of the drive system is not affected. For that, the selected objective of the optimisation process is to improve the overall efficiency and developed torque of the IM. Thus, the multi-objective function is defined as

$$[f] = [f_1 \quad f_2]^T, \tag{23}$$

where f_1 and f_2 are the developed torque, T_d, of (21) and efficiency, η, of (17), respectively. It is important to highlight that the accuracy of the performance model (used to calculate the objective functions) in the optimisation procedure of Fig. 2 is validated using experimental test results, as shown in the Appendix.

The temperature rise problem, which is a crucial parameter in any IM design optimisation activity, is removed by noting the current density in the conductors. Thus, the objective functions of (23) contain constraint functions that are stator J_s and rotor J_r current densities calculated from (15), and are also defined as

$$[g] = [g_1 \quad g_2]^T = [J_s \quad J_r]^T. \tag{24}$$

The current densities in (24) are limited between 4 and 6 A/mm^2 so as to force the solution space to a feasible acceptable design and the ability to cool the motor for the maximum allowable winding temperature, respectively.

Following (7), the multi-objective function of (23) is further defined as a single-objective function given as

$$\text{minimise} \quad f_{\text{R}} = \sum_{m=1}^{2} \epsilon_m^2, \tag{25}$$

where the corresponding residual errors from (7), calculated from the targeted objective function values, are calculated respectively from

$$\epsilon_1 = \begin{cases} 0 & : f_1 \geqslant f_1^{min} \\ \dfrac{f_1^{min} - f_1}{f_1^{min}} & : f_1 < f_1^{min} \end{cases} \quad \text{where } f_1^{min} = 100 \text{ Nm}$$

$$\epsilon_2 = \begin{cases} 0 & : f_2 \geqslant f_2^{min} \\ \dfrac{f_2^{min} - f_2}{f_2^{min}} & : f_2 < f_2^{min} \end{cases} \quad \text{where } f_2^{min} = 99\%. \tag{26}$$

From (26), 100 Nm and 99% are chosen as the exaggerated targeted developed torque and efficiency, respectively, which the MMFD optimiser is forced to achieve. Thus, MMFD optimisation of the IM is achieved by combining T_d and η objective functions into the single-objective function of the sum of squared residual errors, f_{R}, of (25).

TABLE III
MMFD OPTIMISATION RESULTS

case	total iterations	ϵ_1	ϵ_2	f_R
CI	11	0.26120	0.12091	0.08284
C2	10	0.80867	0.21984	0.70228
C3	11	0.93902	0.22038	0.93032
	9	0.22324	0.12271	0.06489
	6	0.22145	0.12379	0.06436

Table III gives the values of the minimised functions of (25), together with the residual error components ϵ_1 and ϵ_2 of (26). These result values are obtained within a few iterations (fewer than eleven iterations, Table III), which shows the robustness of the optimisation procedure from the time-efficient point of view. It can be observed from the results of Table III that the effect of using different initial design values (C1-C3 as of (8)) results in different optimum results, i.e. f_R values in Table III. The acceptable returned solutions every time in Table III demonstrate the capacity of the optimiser in designing the IM geometry and satisfying the design requirements using the derived formulations. According to Table III, the optimal solution of f_R is C1 (row highlighted in grey). The C1 optimum results are transferred to the next starting design variables' problem functions, and the optimum MMFD optimisation results after two rounds (1 and 2, Table III) are also given in Table III (row highlighted in red). It is also noted that, as the rounds progress, the optimisation process converges quickly to the optimum solution, i.e. six iterations in round 2, Table III. From the optimal solution (red highlighted row, Table III), ϵ_1 (developed torque residual error) contributed about 76% and ϵ_2 (efficiency residual error) the remaining percentage to the minimisation of f_R. This is expected, since a very large exaggerated target value was set for the developed toque, as given in (26). Thus, despite having the knowledge of the frame-size motor rating of the used D160M frame, it is of greater importance to try and bring out the best motor performance by exaggerating torque and efficiency so as not to satisfy the first condition of (26), i.e. $\epsilon_1 = \epsilon_2 = 0$. The reason for this, to the designer's knowledge, is to not limit the capability of the optimiser.

Similarly, using (6) for scaled objective and constraint function values, the corresponding actual optimum design variables and objective, and the constraint function values, are given in Table IV. Figure 7 shows the isolated resulting optimum FEM model using the design variables given in Table IV. In addition to the simulated results, the power factor calculated from (16) is 0.78. Thus, despite the objective functions being torque and efficiency, the power factor is good for such a size wound-rotor IM. Comparing the results tabulated in Table IV with the performance of the general purpose D160M frame size four-pole 11 kW cage-rotor IM using IEC standard efficiency, the low performance of the wound-rotor is aligned mainly with the poor slot fill factor (c of (12) taken as 0.4) for machines with a lower power level, which is much higher at large power levels. Hence, future

TABLE IV
ACTUAL OPTIMUM DESIGN VARIABLES, OBJECTIVE AND CONSTRANT FUNCTIONS

variable	value	unit	variable	value	unit
x_1	164.5	mm	x_8	2.2	mm
x_2	2.0	mm	x_9	2.0	mm
x_3	1.5	mm	x_{10}	1.9	mm
x_4	1.0	mm	x_{11}	8.9	mm
x_5	6.8	mm	x_{12}	22.0	mm
x_6	21.0	mm	x_{13}	8	-
x_7	0.2	mm	x_{14}	13.6	rad/s
objective	**value**	**unit**	**constraint**	**value**	**unit**
f_1 (T_d)	78.3	Nm	g_1 (J_s)	6	A/mm^2
f_2 (η)	87.0	%	g_2 (J_r)	6	A/mm^2

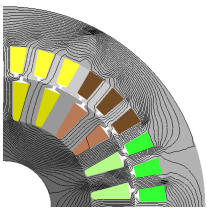

Fig. 7. IM optimum FEM model. phase A, phase B, phase C.

studies of this paper looks at application of the proposed optimisation procedure for large power levels in which skin effects can be perfectly included in the performance model of Fig. 1, using analytical formulae such as in [16]. Despite the slot-fill factor drawback, the application of the optimisation procedure in the design of the WRIM greatly improved the motor torque and efficiency, as given in Table IV. The latter is contrary to the expectation when compared to the considered IE1 frame size cage-rotor IM (nearly a unit rotor slot fill factor) of approximately 74 Nm torque and 87.6% efficiency, although with higher power factor of 0.86 at full load [11].

It can be observed from Fig. 7 that the isolated optimum IM design has deep teeth, resulting in high current densities as tabulated in Table IV. For the increased current densities, both stator and rotor slot aspect ratios (slot height divided by slot width) were less than 3. The latter is to reduce the flux leakages, which resulted in the better power-factor performance of the motor. As earlier stated, given the stack length, the decrease in stator winding turns resulted in an increase of efficiency due to the increased air-gap average flux density at the fixed grid voltage. The latter is observed in Fig. 7, and resulted in an increased stator slot teeth and back core height to accommodate the pole flux. In addition, the resultant rated slip angular frequency (x_{14}) of Table IV explains the low slip angular frequencies that come with high efficiency and the corresponding developed torque, along with the fairly low power factor.

VII. CONCLUSIONS

In this paper, the multi-objective optimisation using MMFD with a computationally efficient parameter and performance method for the solution of the non-linear con-

strained optimisation problem is applied to the optimisation of the grid-connected WRIM design. By presenting results on a small-scale WRIM, the implementation and applicability of the optimisation procedure with torque and efficiency as objective functions are demonstrated. Improved torque and efficiency are achieved using the proposed optimisation procedure. The latter also comes with a motor design with an improved power factor.

The following conclusions are drawn from the optimal solution results:

- the gradient-based optimiser is effective and powerful for practical multi-objective optimisation problems if the interface model quality is improved;
- although the optimisation problem function does not qualify the requirements of linearity, the results of the quality formulated functions demonstrate the robustness and ruggedness of the formulated optimisation procedure;
- from the results, it can be noticed that if the factors affecting the optimisation problem function are properly taken care of, the global optimum can be achieved in very few exploratory;
- the reduced computational effort using the gradient-based optimiser facilitates the optimisation of the complex structure of the IM, hence the IM can be designed in a simple optimisation process using modern finite element methods; and
- the optimisation procedure using the gradient-based optimiser allows the imposition of minimum and maximum multi-objective functions explicitly without any additional complexity.

VIII. Appendix

Figure 8 depicts the measured and calculated performance characteristics of a four-pole, 400V/50Hz existing grid-connected IM. The latter shows the accuracy of the performance model in Fig. 2 using experimental measurements for validation.

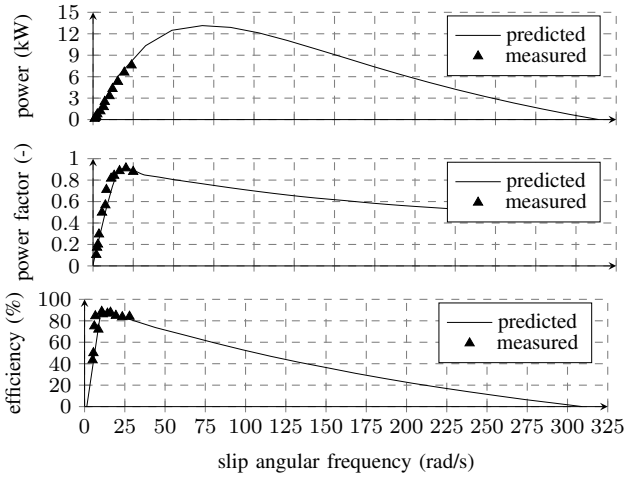

Fig. 8. IM predicted and measured performance characteristics.

References

[1] B. Amin, *Induction motors: analysis and torque control*. Springer Science & Business Media, 2001.

[2] D. Hong, J. Choi, D. Kim, Y. Chun, B. Woo, and D. Koo, "Development of a high speed induction motor for spindle systems," *IEEE Transactions on Magnetics*, vol. 49, no. 7, pp. 4088–4091, July 2013.

[3] N. Riviére, M. Villani, and M. Popescu, "Optimisation of a high speed copper rotor induction motor for a traction application," in *IECON 2019 - 45th Annual Conference of the IEEE Industrial Electronics Society*, vol. 1, 2019, pp. 2720–2725.

[4] M. Mabhula and M. J. Kamper, "Computational efficient parameter and performance prediction of wound-rotor induction motor," *IEEE Transactions on Magnetics*, vol. 54, no. 6, pp. 1–7, 2018.

[5] P. Alotto and M. A. Nervi, "An efficient hybrid algorithm for the optimization of problems with several local minima," *International Journal for Numerical Methods in Engineering*, vol. 50, no. 4, pp. 847–868, 2001.

[6] X. Yu and M. Gen, *Introduction to Evolutionary Algorithms*, ser. Decision Engineering. Springer London, 2010.

[7] Linxia Guo, Yu Cheng, Lizi Zhang, and Haitao Huang, "Research on power factor regulating tariff standard," in *2008 China International Conference on Electricity Distribution*, December 2008, pp. 1–5.

[8] I. Boldea and S. Nasar, *The Induction Machine Handbook*, ser. Electric Power Engineering Series. CRC Press, 2010.

[9] N. R. Kulkami, H. V. Murthy, and A. P. Raju, "Plc based intelligent power factor correctors for industrial power systems-a case study," in *2015 International Conference on Power and Advanced Control Engineering (ICPACE)*, August 2015, pp. 75–79.

[10] Y. Kabir, Y. M. Mohsin, and M. M. Khan, "Automated power factor correction and energy monitoring system," in *2017 Second International Conference on Electrical, Computer and Communication Technologies (ICECCT)*, February 2017, pp. 1–5.

[11] ABB Motors and Generators, "Low voltage general performance motors," Catalog, December 2017. [Online]. Available: https://www.baldor.com/mvc/DownloadCenter/Files/9AKK105789

[12] M. Mabhula, "Analysis and design optimisation of grid-connected wound-rotor synchronous and induction motors," PhD dissertation, Stellenbosch University, December 2019.

[13] Vanderplaats Research and Development, Inc, ""VisualDOC: Software for Process Integration and Multidiscipline Design Optimization"," June 2008, aceessed June, 30, 2019. [Online]. Available: http://www.vrand.com/products/visualdoc/

[14] G. Venter, *Review of Optimization Techniques*. John Wiley and Sons, Ltd, 2010.

[15] M. Kamper, "Design optimisation of cageless flux barrier rotor reluctance synchronius machine," PhD dissertation, Stellenbosch University, December 1996.

[16] J. Lammeraner and M. Štafl, *Eddy Currents [by] Jiří Lammeraner and Miloš Štafl. English Translation Edited by G.A. Toombs [Translated by Miloš Štafl].*, 1966.

IX. Biographies

Mkhululi Mabhula received the BEng and PhD (Eng), MSc upgraded degrees from Stellenbosch University, South Africa in 2016 and 2019, respectively. He is currently doing his post-doctoral research in electrical machine design. His main interest is the design optimisation and control of electrical machines.

Maarten J. Kamper received the MSc. (Eng) and PhD (Eng) degrees from the University of Stellenbosch in South Africa in 1987 and 1996, respectively. Since 1989, he has been with the Department of Electrical and Electronic Engineering at the university, where he is currently a professor of electrical machines and drives. His research interests includes design optimisation and control of electrical machines, currently with a focus on wind generators and industrial and electrical vehicle drives. Prof. Kamper is a South African National Research Foundation-supported scientist and a registered Professional Engineer in South Africa.